GWO-SUPER-TWISTING INTEGRAL SLIDING MODE CONTROL OF 60 KW PV SYSTEM BASED ON INTERLEAVED BOOST CONVERTER

Daia Eddine Oussama Mohamed Cherif [1] – Ali Chebabhi[2] – Abdelhalim Kessal[1*] – Mohammed Karim Fellah[3] – Mohamed-Fouad Benkhoris[4]

[1] LPMRN Laboratory, Faculty of Sciences & Technology, University Mohammed El Bachir El Ibrahimi of Bordj Bou Arreridj, Algeria.
[2] EE Laboratory, Department of Electrical Engineering, Faculty of Technology, University of M'sila, Algeria.
[3] ICEPS Laboratory (Intelligent Control & Electrical Power Systems), Djillali Liabes University of Sidi Bel-Abbes. Algeria.
[4]IREENA Laboratory (Institut de Recherche en Energie Electrique de Nantes Atlantique), University of Nantes, Saint-Nazaire, France.

ARTICLE INFO

***Article history*:**
Received:
Received in revised form:
Accepted:

Keywords:
Super twisting algorithm (STA)
Integral sliding mode control (ISMC)
Interleaved boost converter (IBC)
Grey wolf optimizer (GWO)
Photovoltaic (PV)

DOI: https://doi.org/10.30765/er.2167

Abstract:

The energy provided by the PV system is strongly influenced by climatic conditions such as solar radiation and cell temperature. A suitable DC /DC converter and a robust control strategy combined with the maximum power point tracking (MPPT) algorithm are required to harness the maximum power of the panel. This paper proposes a super-twisting integral sliding mode control (ST-ISMC) for four legs interleaved boost converter (FLIBC) as an interface to the MPPT algorithm for a 60 KW PV system. The FLIBC has been used to overcome the drawbacks of the conventional boost converter (CBC). The ST-ISMC is proposed to maintain the PV voltage track the reference provided by the MPPT algorithm and ensure the equal sharing of input current between legs. The controller gains of the proposed ST-ISMC have been calculated using the grey wolf optimization algorithm for better performance. The simulation results prove the excellent performance of the proposed controller over the conventional controller.

1 Introduction

Nowadays, due to global warming, the world needs pollution-free energy sources such as solar, geothermal, hydropower, and wind to meet the growing electricity demand [1], [2]. These sources are accessible, clean, sustainable, inexhaustible, and pollution-free. The use of renewable energy in daily life has become a significant challenge for researchers and engineers.

The photovoltaic system is one of the most dominant ways to harvest solar energy, where solar radiation is directly converted to electricity. The electrical characteristics of the PV panel, such as the power voltage (P-V) and the current voltage (I-V), are nonlinear and depend on the climatic conditions [3]. For each irradiance and temperature, there is only one point on the P-V curve, called the MPP, at which maximum power is reached. Variations in irradiance and temperature change the MPP, which makes obtaining maximum PV power an exciting challenge for researchers.

Many solutions have been proposed in the literature to exploit the maximum power of PV panels using Maximum Power Point Tracking (MPPT) [4]- [10]. The execution of MPPT technique requires the use of a DC-DC converter; the boost converter is a widely used topology as an interface between the PV panel and the

* Corresponding author
E-mail address: abdelhalim.kessal@univ-bba.dz

load. However, the conventional boost converter (CBC) has drawbacks such as power ripple, low efficiency, and high voltage stress [11]. In various works, such as [12] and [13], an interleaved topology consisting of multiple identical boost converters connected in parallel is proposed. The researchers point out the benefits such as low power ripple, high efficiency, high power conversion, and low voltage stress on the components [14]. Saidj et al [15] use accurate operational tests to assess and compare the overall performance of the IBC architecture with the CBC. The results show that the interleaved topology can significantly increase efficiency while reducing output power ripple, switching losses, and heat dissipation. In [8], Farh et al. proposed an efficient solution using the IBC and the P&O MPPT algorithm to utilize the maximum power of a partial shading system. The results of the study have shown that the IBC ensures that the full power is obtained from the partially shaded PV system, which cannot be accomplished using CBC topology. An IBC is used with the current sensorless MPPT technique to obtain the maximum power from the PV system studied in [16]. However, the previous work uses unstable control methods and miss the robustness when disturbances are introduced into the system. Conversely, a reliable controller must be used to evenly divide the input current to avoid excessive current and heating that destroys the components.

Numerous control techniques have been proposed to solve the technical challenges. In [17]- [19], a dual-loop controller PI is proposed to control an IBC. However, linear control strategies may lead to a lack of system robustness. Moreover, they are unsuitable for controlling PV systems with IBCs due to their nonlinear behaviour. Therefore, researchers propose various nonlinear strategies to overcome the drawbacks of linear controllers. In [20], a finite control set was studied in which the controller uses the predicted behaviour of the IBC and selects the optimal switching state by minimising the cost function. Vargas-Gil et al. proposed a fixed switching frequency controller in sliding mode (SMC) plus PI for the input voltage of a two- phase IBC connected to PV panels [21]. Compared with the lead-lag controller, the proposed strategy shows a robust response in the presence of a sudden change in ambient conditions. However, flutter is a significant problem in 1st order SMC, which causes heat loss in the power converter. Super-twisting sliding mode control (ST-SMC) has been extensively studied in various applications [22], [23]. In [24], a ST-SMC was developed for MPPT control of a PV system based on a noninverting buck converter to gain maximum power. Chattering was eliminated and the dynamic response of the overall system was improved compared to SMC and synergetic controller.

In this paper, an integral super-twisting sliding mode control system (ST-ISMC) of a 60KW PVS based on FLIBC is investigated. The proposed configuration of the PVS in conjunction with FLIBC can be enhanced by using a robust nonlinear control based on ST-ISMC. The proposed controller consists of double loop controllers. The outer loop consists of ST-ISMC for controlling the input voltage of the PVS, which is used to maintain the PV voltage trace and the MPP voltage supplied by the MPPT algorithm and eliminate the steady state error. The PI controller is used as an inner loop to ensure the input current is evenly distributed among the legs. The GWO algorithm is used to find the optimal gain of the proposed ST-ISMC. Extensive simulations are performed in the MATLAB/Simulink environment to verify the effectiveness of the proposed controller and demonstrate its superiority over the ST-SMC, SMC and PI controllers.

The rest of this paper is organized as follows: Section 2 describes and models the proposed topology. In Section 3, the ST-ISMC is discussed and described in detail. Simulation results and performance validation using MATLAB/Simulink are presented in Section 4; and finally, Section 5 concludes the paper.

2 Four legs interleaved boost converter topology and modelling

Figure 1 depicts the proposed system in detail. It comprises of PV array connected with a resistance acting as a load through the FLIBC.

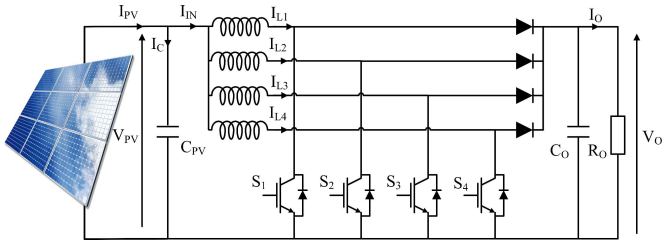

Figure 1. Standalone PV system based on FLIBC.

2.1 Photovoltaic panel module

Solar cells are p-n junction semiconductors. When light is incident, a photocurrent is generated. The one-diode equivalent circuit is the most commonly used PV module [25], which consists of an ideal parallel diode with a current source, a series resistor representing the internal cell resistance, and a shunt resistor representing the losses due to diode leakage current (see Figure 2). Equation 1 represents a PV module developed with a single diode model. Table 1 lists the PV panel parameters used in the simulation.

$$I = I_{ph} - I_0\left[\exp\left(\frac{V_{PV} + R_S I_{PV}}{\alpha V_T}\right) - 1\right] - \left(\frac{V_{PV} + R_S I_{PV}}{R_P}\right) \quad (1)$$

where

I_{ph}: Photo-current generated by PV cell.
I_0: The reverse saturation current of the diode.
I_{PV}: Current generated by PV cell.
V_{PV}: Voltage at the terminals of the PV cell.
V_T: Thermal voltage of PV cell.
R_S: The equivalent series resistance.
R_P: The equivalent parallel resistance.
α: Diode ideality factor.

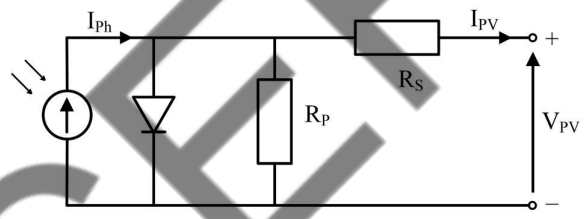

Figure 2. PV single diode module equivalent circuit.

Table 1. PV panel specifications.

Parameter	Symbol	Value
Open circuit voltage [V]	V_{OC}	21.83
Short circuit current [A]	I_{SC}	5.33
The voltage at the maximum power point [V]	V_{MPP}	17.27
Current at the maximum power point [A]	I_{MPP}	4.93
Maximum power [w]	P_{MPP}	85.14
reverse saturation current of the diode [A]	I_0	$4.9414x10^{-10}$
Diode ideality factor	α	1.0227
Parallel resistance [Ω]	R_P	149.63
Series resistance [Ω]	R_S	0.3749

2.2 Four legs interleaved boost converter

In the literature study, a four-legged nested up-converter is proposed for a PV system to solve the mentioned CBC constraints [26], as shown in Figure 1. It consists of four conventional boost converters connected in parallel with the same switching frequency and a quarter period as the phase shift between each branch. The differential equations describing the operating dynamics of the FLIBC based on the state of the switches (S1, 2, 3, 4) and using Kirchhoff's voltage and current law can be given as follows:

$$\begin{cases} C_{PV}\dfrac{dV_{PV}(t)}{dt} = I_{PV}(t) - I_{IN}(t) \\ L\dfrac{dI_{Lj}(t)}{dt} = V_{PV}(t) - (1-S_j)V_o(t) \end{cases} \quad (2)$$

V_{PV}, I_{PV}, I_{IN}, V_o, and I_{Lj} are the PV panel's voltage, the PV panel's current, the FLIBC input current, the FLIBC output voltage, and the phase current, respectively. In addition, $L=L_1= L_2= L_3= L_4$ is the value of the inductor of each leg. Then, the FLIBC average model can be expressed as follows:

$$\begin{cases} C_{PV}\dfrac{dV_{PV}(t)}{dt} = I_{PV}(t) - I_{IN}(t) \\ L\dfrac{dI_{Lj}(t)}{dt} = V_{PV}(t) - (1-D_j)V_o(t) \end{cases} \quad (3)$$

D_j is the average value of S_j, called the duty cycle.

3 Control approach

A dual loop controller is proposed to effectively track the reference voltage provided by an MPPT algorithm for each value of solar irradiation and temperature to extract maximum power from the PV panels. A nonlinear robust super-twisting integral sliding mode control is suggested as an outer loop controller to regulate the voltage of PV panels. A PI controller is used as inner loop control to ensure the equal sharing of FLIBC input current between the legs. The controller parameters are tuned using a particle swarm optimization algorithm by minimization of a cost function that minimizes the tracking error.

3.1 Proposed super-twisting integral sliding mode control (ST-ISMC)

ST-ISMC is commonly used to eliminate the traditional SMC drawbacks. It shows a significant superiority against disturbances and overshot compared to SMC [27]. To extract the maximum power from the PV panels must maintain the PV voltage V_{PV} track the reference voltage V_{PVref} provided by the MPPT algorithm. Where the voltage tracking error and sliding surface are defined, respectively as

$$e_V(t) = V_{PVref}(t) - V_{PV}(t) \quad (4)$$

$$S_V(t) = e_V(t) + \lambda\int_0^t e_V(t)dt \quad (5)$$

where λ must be a definite positive constant. Therefore, the derivative of the proposed sliding surface can be given as

$$\dot{S}_V(t) = \dot{e}_V(t) + \lambda\, e_V(t) = \dot{V}_{PVref}(t) - \dot{V}_{PV}(t) + \lambda\, e_V(t) \quad (6)$$

Then, using the differential equations of FLIBC Eq. (3), Eq. (6) rewritten as

$$\dot{S}_V(t) = \dot{V}_{PVref}(t) - \frac{1}{C_{PV}}\left(I_{PV}(t) - I_{IN}(t)\right) + \lambda\, e_V(t) \quad (7)$$

Therefore, the FLIBC input current I_{IN} will be the control term in which the PV panel voltage will be regulated by considering the FLIBC input current as a reference to the inner loop controller. In addition, the control law of ST-ISMC given as

$$I_{IN} = I_{IN-eq} + I_{IN-ST} \tag{8}$$

The equivalent control part $I_{IN\text{-}eq}$ can be deduced through the equation as follows:

$$I_{IN-eq} = -C_{PV}\left(\dot{V}_{PVref}(t) + \lambda\, e_V(t)\right) + I_{PV}(t) \tag{9}$$

And based on the ST algorithm $I_{IN\text{-}ST}$, the discontinues control part can be obtained as

$$\begin{cases} I_{IN-ST} = -\alpha_V \left|S_V(t)\right|^{\frac{1}{2}} \operatorname{sgn}\left(S_V(t)\right) + u \\ \dot{u} = -\beta_V \operatorname{sgn}\left(S_V(t)\right) \end{cases} \tag{10}$$

where α_V and β_V are the controller gains and can be calculated by using the following equations

$$\begin{cases} \beta_V > \dfrac{\Psi}{\Gamma_M} \\ \alpha_V \geq \dfrac{4\Psi\Gamma_M(\beta_V + \Psi)}{\Gamma_m^3(\beta_V - \Psi)} \end{cases} \tag{11}$$

where Ψ define the positive bounds of the uncertain function φ, Γ_M and Γ_m are the upper and lower positive bounds of the uncertain function ϕ at the second derivative of the sliding manifold [27].

$$\Psi > \varphi \text{ and } \Gamma_M \geq \phi \geq \Gamma_m \tag{12}$$

$$V_{PV} = \varphi(x,t) + \phi(x,t)\dot{I}_{IN} \tag{13}$$

On the other hand, the open loop transfer function of the inner loop is required to design the FLIBC input current controller to ensure the equal sharing of the current among the legs. And can be deduced from (3) as

$$F(s) = \frac{I_{IN}(s)}{U(s)} = \frac{1}{Ls} \tag{14}$$

where

$$U(s) = V_{PV}(s) - (1 - D_j)V_o(s) \tag{15}$$

The transfer function of the PI controller used as an inner loop controller to ensure the equal sharing of the input current among the legs is given as

$$PI(s) = K_P + \frac{K_i}{s} \tag{16}$$

Therefore, the closed-loop transfer function is written as follows:

$$G(s) = \frac{K_P s + K_i}{s^2 + \dfrac{K_P}{L}s + \dfrac{K_i}{L}} \tag{17}$$

Then, based on the canonical form of second order system, the PI controller gains can be written as

$$\begin{cases} K_P = 2\xi\omega L \\ K_i = L\omega^2 \end{cases} \tag{18}$$

where ξ and ω, respectively, are the damping ratio and cut-off frequency of the PI controller. In Figure 3, the block diagram of the proposed control method has been illustrated.

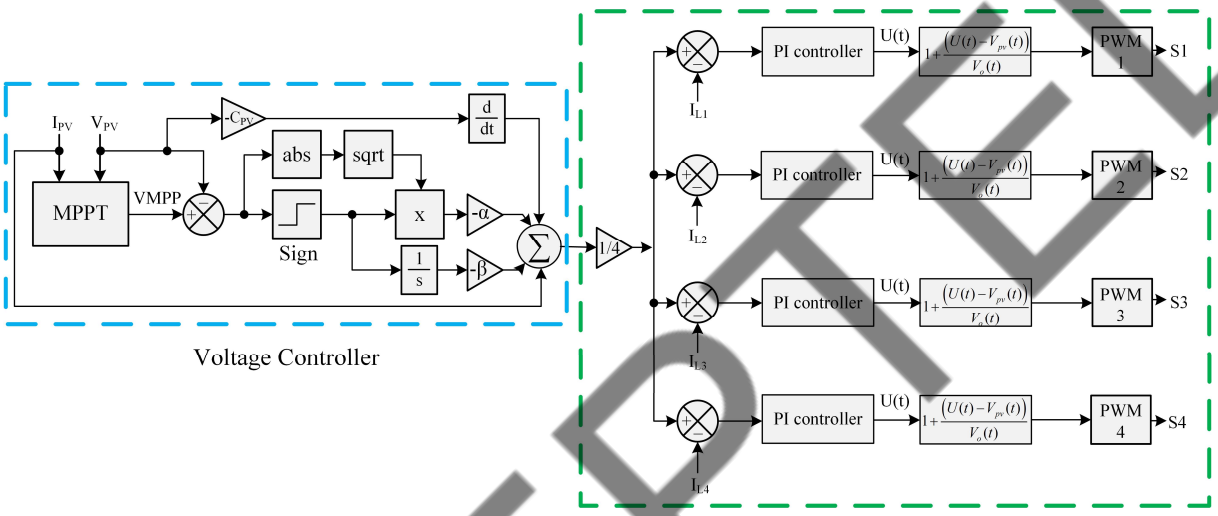

Figure 3. Block diagram of the proposed control method.

3.2 Grey wolf optimization algorithm

The social structure and hunting strategy of grey wolves in nature inspire the Grey Wolf Optimizer (GWO) [28], which is an optimization algorithm. It employs four kinds of wolves: alpha, beta, delta, and omega, to represent the leadership and collaboration among the wolves. The algorithm also follows the three main phases of hunting: searching for prey, encircling prey, and attacking prey [29]. The GWO algorithm can handle various optimization problems with unknown search spaces [28].

The following mathematical equations describe the hunting procedures mentioned above:

$$\vec{D} = \left|\vec{C}.\vec{X}_p(i) - \vec{X}(i)\right| \tag{19}$$

$$\vec{X}(i+1) = \left|\vec{X}_P(i) - \vec{A}.\vec{D}\right| \tag{20}$$

where X_P is the position vector of the prey, i is the recent iteration, X is the vector of the grey wolves' position, D is a vector that refers to the distance between the prey and wolves, and A and C are coefficient vectors which can be computed using the following equations

$$\vec{C} = 2\vec{r}_1 \tag{21}$$

$$\vec{A} = 2\vec{a}\vec{r}_2 - \vec{a} \tag{22}$$

r_1 and r_2 are the random numbers that vary in each iteration among the range [0, 1]. In addition, a is vector decreased during iterations from 2 to 0. According to the grey level, the distance of each level can be given as

$$\begin{cases} \vec{D}_\alpha = \left|\vec{C}_1.\vec{X}_\alpha - \vec{X}\right| \\ \vec{D}_\beta = \left|\vec{C}_2.\vec{X}_\beta - \vec{X}\right| \\ \vec{D}_\delta = \left|\vec{C}_3.\vec{X}_\delta - \vec{X}\right| \end{cases} \quad (23)$$

where D_α, D_β, and D_δ are the distances between wolves of alpha level and prey, wolves of beta level and prey, and wolves of delta level and prey. C_1, C_2, and C_3 are the coefficient vectors of the first three best fittest positions X_1, X_2, and X_3. And X_α, X_β, and X_δ are the best search agents. The equations that represent the three best positions of grey wolves are expressed in (24)

$$\begin{cases} \vec{X}_1 = \vec{X}_\alpha - \vec{A}_1(\vec{D}_\alpha) \\ \vec{X}_2 = \vec{X}_\beta - \vec{A}_2(\vec{D}_\beta) \\ \vec{X}_3 = \vec{X}_\delta - \vec{A}_3(\vec{D}_\delta) \end{cases} \quad (24)$$

The formula below can be used to compute the position of the prey for the best search agent

$$\vec{X}(i+1) = \frac{\vec{X}_1 + \vec{X}_2 + \vec{X}_3}{3} \quad (25)$$

Then, the proposed objective function is formulated based on the integral time square error value, which is defined as follows:

$$ITSE = \int_0^t t(V_{PVref} - V_{PV})^2 \, dt \quad (26)$$

The pseudo-code of the grey wolf optimizer algorithm is shown in Table 2.

Table 2. The GWO algorithm pseudo-code.

```
1. Initialize a population of N wolves randomly
2. Evaluate the fitness of each wolf
3. Identify alpha, beta, and gamma wolves (the best three wolves)
4. Set a as a linearly decreasing parameter from 2 to 0
5. Set iteration counter t = 0
6. While t < maximum number of iterations do
     For 1:N
       Calculate A and C vectors using random numbers
       Calculate D vectors for alpha, beta, and gamma wolves using A, C, and the positions of the wolves
       Calculate X vectors for alpha, beta, and gamma wolves using D and the positions of the wolves
       Calculate the new position of the current wolf as the average of X vectors
        Apply boundary conditions if necessary
     End for
     Update alpha, beta, and gamma wolves (the best three wolves)
     Update a parameter
     Update iteration counter t = t + 1
End while
7. Return alpha wolf as the best solution
```

4 Simulation Results and Discussion

The proposed system with a 60 Kw PV system based on FLIBC and a controller with optimised ST-ISMC, tuned with the GWO algorithm, is modelled and simulated using MATLAB/Simulink. The simulation parameters are listed in Table 3. The system was tested under sudden irradiance variations to verify the

robustness and reliability of the proposed system (see Figure 4), and at constant temperature (25 °C). The solar radiation regarded was initially 800 W/m² and varied with time.

Figure 5 illustrates the behaviour of the PV voltage when the irradiation level changes with different controllers. It can be observed that the proposed strategy GWO-ST-ISMC has a better dynamic behaviour and the PV voltage follows the reference voltage with less variation. Compared to the other controllers, the settling time with GWO-ST-ISMC has decreased from 10 ms to 1.40 ms. Also, the overshoot has decreased from 6.80% to 0.27%. When the irradiance changed suddenly from 1000 w/m² to 200 w/m², the maximum power point voltage was tracked quickly with less overshoot. The obtained data are summarised in Table 4. *Table 3. Simulation parameters.*

FLIBC Parameters	**Value**
$L=L_1=L_2=L_3=L_4$	5 mH
C_{PV}	63 uF
C_o	33 uF
R_o	324 Ω
Switching frequency	50 kHz
Series PV panels	48
Parallel PV panels	15
GWO Parameters	
Population of wolves	20
Max iteration	30

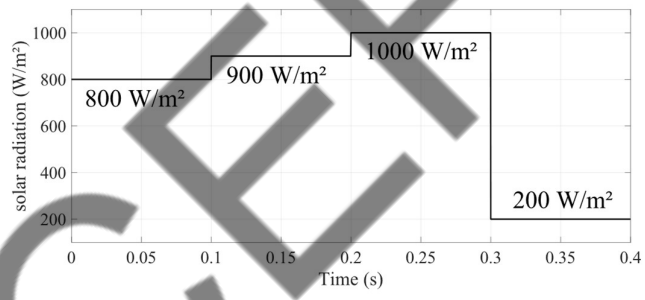

Figure 4. Solar irradiation profile used in the simulation.

Figure 6 illustrates the PV panels obtained using GWO-ST-ISMC. It can be seen that the current reference is tracked successfully using the proposed controller with a fast response and less overshoot compared to the other controllers. Moreover, the GWO-ST-ISMC provides excellent performance regarding the chattering problem; the peak power of the PV system is tracked without fluctuations, as depicted in Figure 7. Thus, the efficiency is enhanced.

The current curve of the legs is shown in Figure 8. The equal sharing of the current among legs is achieved thanks to the current control loop. That operation reduces the ripples and voltage stress of the switches and increases the power converted.

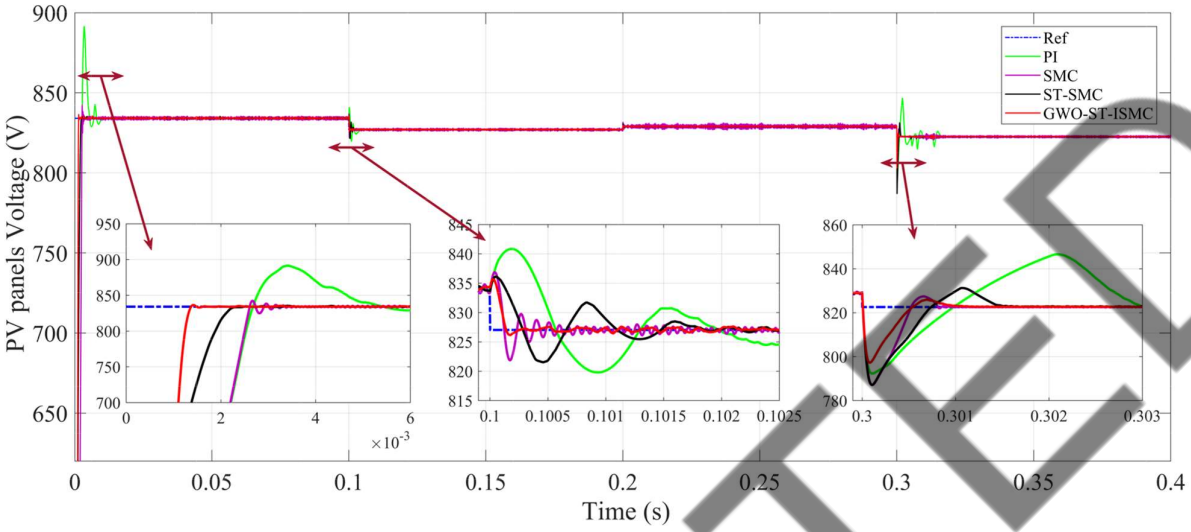

Figure 5. The PV panels voltage curve under solar irradiation.

Table 4. summarizes data on PV voltage.

Solar radiation step		Settling time (ms)				Overshoot (%)			
Start	**End**	**PI**	**SMC**	**ST-SMC**	**GWO-ST-ISMC**	**PI**	**SMC**	**ST-SMC**	**GWO-ST-ISMC**
0	0.1	10	3	2.3	1.4	6.80	0.98	0.24	0.27
0.1	0.2	4.3	0.6	1.1	0.1	1.16	1.12	1.11	1.03
0.2	0.3	1.2	0.5	0.2	0.1	0.20	0.31	0.20	0.06
0.3	0.4	11	0.7	1.4	0.5	2.91	0.58	1.04	0.40

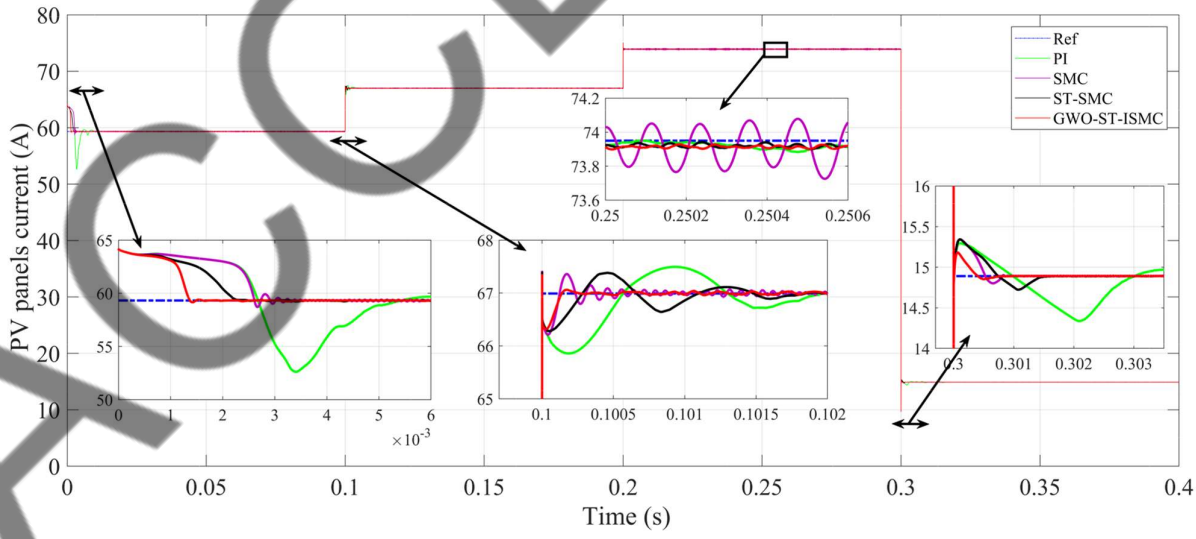

Figure 6. The PV panel's current curve during the solar irradiation step changes.

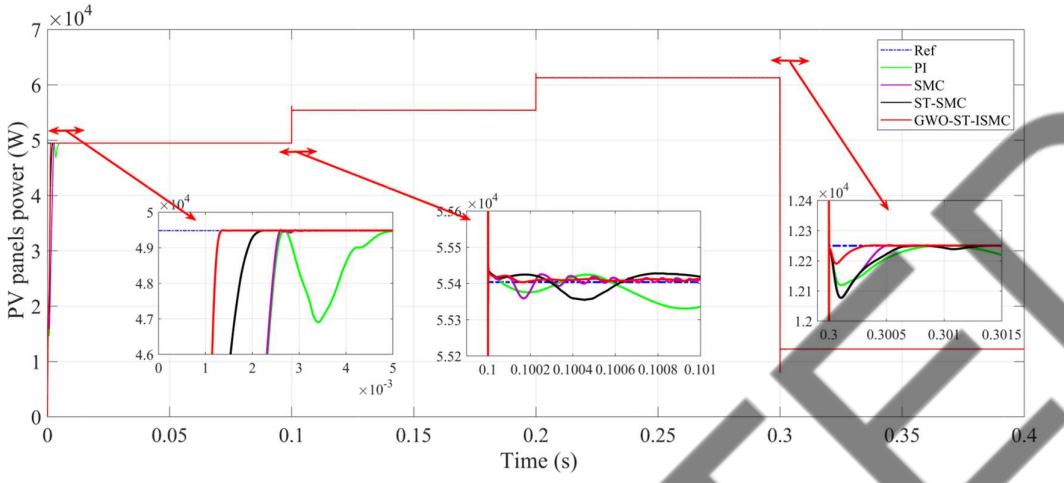

Figure 7. PV power during sudden irradiation variation.

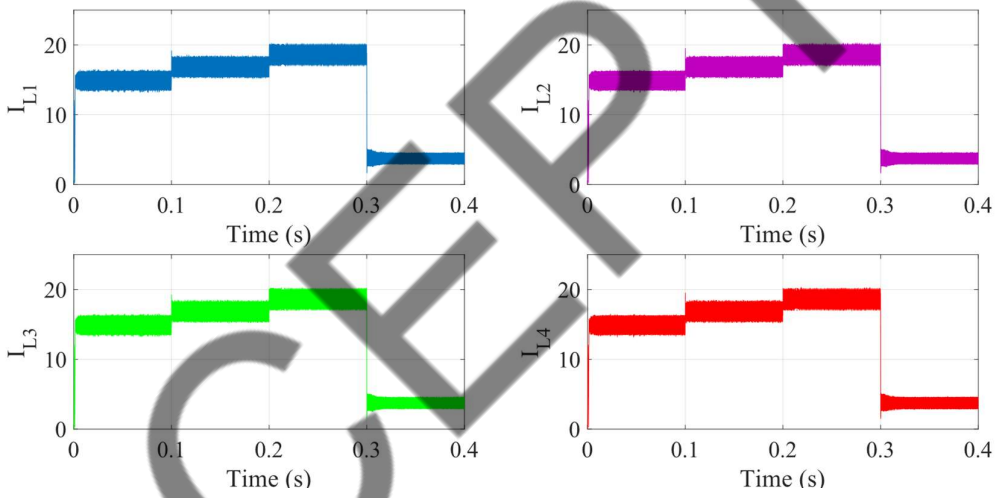

Figure 8. The inductors' current curves.

The control strategies' performance is evaluated using performance indices such as integral absolute error (IAE), integral square error (ISE), integral time absolute error and integral time square error (ITSE). Table 5 compares the proposed strategy with other control techniques using these indices. It can be observed that GWO-ST-ISMC has a better performance compared to other control strategies.

Table 5. Comparison of the performance indices.

Control Strategies	Performance Indices			
	IAE	ISE	ITAE	ITSE
PI Controller	1.2540	526	0.032520	0.6645
SMC	1.2080	516.3	0.038550	0.4770
ST-SMC	0.7316	339.4	0.011860	0.2526
GWO-ST-ISMC	0.5978	295.9	0.008569	0.1243

5 Conclusion

In this paper, an improved PV system considering the optimized ST-ISMC is proposed to control a FLIBC. The control strategy used to maintain the PV voltage follows the reference established by the MPPT algorithm

and ensures the uniform distribution of the input current among the legs. Moreover, the controller gains were tuned using the GWO algorithm to achieve the best performance. Simulation results under sudden climatic conditions demonstrate the superiority of the proposed system in terms of maximum power tracking speed, zero steady state error, reduced chattering, and lower overshoot. Moreover, the system operates in a wide power range that allows to increase the efficiency of the PV panels by 99.8%. For future work, we propose to use nonlinear control to replace the PI inner loop controller and use adaptive control approaches to deal with the external disturbances affecting the system.

References

[1] D. K. Dhaked and D. Birla, "Modeling and control of a solar-thermal dish-stirling coupled PMDC generator and battery based DC microgrid in the framework of the ENERGY NEXUS," *Energy Nexus*, vol. 5, p. 100048, Mar. 2022, doi: 10.1016/j.nexus.2022.100048.

[2] N. Priyadarshi *et al.*, "Performance Evaluation of Solar-PV-Based Non-Isolated Switched-Inductor and Switched-Capacitor High-Step-Up Cuk Converter," *Electronics*, vol. 11, no. 9, p. 1381, Apr. 2022, doi: 10.3390/electronics11091381.

[3] Z. Wang, Y. Li, K. Wang, and Z. Huang, "Environment-adjusted operational performance evaluation of solar photovoltaic power plants: A three stage efficiency analysis," *Renew. Sustain. Energy Rev.*, vol. 76, pp. 1153–1162, Sep. 2017, doi: 10.1016/j.rser.2017.03.119.

[4] J. Ahmed and Z. Salam, "An Enhanced Adaptive P&O MPPT for Fast and Efficient Tracking Under Varying Environmental Conditions," *IEEE Trans. Sustain. Energy*, vol. 9, no. 3, pp. 1487–1496, 2018, doi: 10.1109/TSTE.2018.2791968.

[5] S. Nahar, M. R. Ahmed, and A. Afrin, "Performance Analysis of Solar MPPT (InC Algorithm) Based Three Phase Interleaved Boost Converter using Coupled Inductor for Brushless DC Motor," in *2018 International Conference on Advancement in Electrical and Electronic Engineering (ICAEEE)*, Nov. 2018, pp. 1–4. doi: 10.1109/ICAEEE.2018.8643000.

[6] B. P. Ganthia, R. Pradhan, S. Das, and S. Ganthia, "Analytical study of MPPT based PV system using fuzzy logic controller," in *2017 International Conference on Energy, Communication, Data Analytics and Soft Computing (ICECDS)*, Aug. 2017, vol. 49, no. 598, pp. 3266–3269. doi: 10.1109/ICECDS.2017.8390063.

[7] M. Kermadi and E. M. Berkouk, "Artificial intelligence-based maximum power point tracking controllers for Photovoltaic systems: Comparative study," *Renew. Sustain. Energy Rev.*, vol. 69, no. February 2019, pp. 369–386, Mar. 2017, doi: 10.1016/j.rser.2016.11.125.

[8] H. M. H. Farh, A. M. Eltamaly, and M. S. Al-Saud, "Interleaved boost converter for global maximum power extraction from the photovoltaic system under partial shading," *IET Renew. Power Gener.*, vol. 13, no. 8, pp. 1232–1238, 2019, doi: 10.1049/iet-rpg.2018.5256.

[9] M. R. Mostafa, N. H. Saad, and A. A. El-sattar, "Tracking the maximum power point of PV array by sliding mode control method," *Ain Shams Eng. J.*, vol. 11, no. 1, pp. 119–131, 2020, doi: 10.1016/j.asej.2019.09.003.

[10] C. Gonzalez-Castano, C. Restrepo, S. Kouro, and J. Rodriguez, "MPPT Algorithm Based on Artificial Bee Colony for PV System," *IEEE Access*, vol. 9, pp. 43121–43133, 2021, doi: 10.1109/ACCESS.2021.3066281.

[11] K. A. Singh, A. Prajapati, and K. Chaudhary, "High-Gain Compact Interleaved Boost Converter With Reduced Voltage Stress for PV Application," *IEEE J. Emerg. Sel. Top. Power Electron.*, vol. 10, no. 4, pp. 4763–4770, Aug. 2022, doi: 10.1109/JESTPE.2021.3120802.

[12] G. G. Ramanathan and N. Urasaki, "Non-Isolated Interleaved Hybrid Boost Converter for Renewable Energy Applications," *Energies*, vol. 15, no. 2, p. 610, Jan. 2022, doi: 10.3390/en15020610.

[13] P. R. Sarkar, A. K. Yadav, A. F. Minai, and R. K. Pachauri, "MPPT Based SPV System Design and Simulation Using Interleaved Boost Converter," in *2021 International Conference on Control, Automation, Power and Signal Processing (CAPS)*, Dec. 2021, vol. 1, pp. 1–6. doi: 10.1109/CAPS52117.2021.9730712.

[14] G. Liu, M. Wang, W. Zhou, Q. Wu, and Y. Fu, "A Sensorless Current Balance Control Method for Interleaved Boost Converters Based on Output Voltage Ripple," *IEEE Trans. Power Electron.*, vol. 36, no. 6, pp. 7138–7149, Jun. 2021, doi: 10.1109/TPEL.2020.3037650.

[15] S. H. Saidj, S. Boumechta, A. Degla, A. Djoudi, A. H. Arab, and M. Haddadi, "Comparison and Experimental Tests between Conventional and Interleaved DC/DC Boost Converter Topology," in *2020 6th International Symposium on New and Renewable Energy (SIENR)*, Oct. 2021, pp. 1–5. doi: 10.1109/SIENR50924.2021.9631894.

[16] E. A. Tonolo, J. W. M. Soares, E. F. R. Romaneli, and A. A. Badin, "Current Sensorless MPPT With a CCM Interleaved Boost Converter for Renewable Energy System," *IEEE Trans. Power Electron.*, vol. 37, no. 9, pp. 11296–11304, 2022, doi: 10.1109/TPEL.2022.3166747.

[17] M. W. Ahmad, N. B. Y. Gorla, H. Malik, and S. K. Panda, "A Fault Diagnosis and Postfault Reconfiguration Scheme for Interleaved Boost Converter in PV-Based System," *IEEE Trans. Power Electron.*, vol. 36, no. 4, pp. 3769–3780, Apr. 2021, doi: 10.1109/TPEL.2020.3018540.

[18] M. C. Daia Eddine O, A. Chebabhi, and A. Kessal, "Four leg Interleaved DC/DC boost Converter based PV system using PSO Algorithm based PI controller," in *2022 19th International Multi-Conference on Systems, Signals & Devices (SSD)*, May 2022, pp. 1415–1421. doi: 10.1109/SSD54932.2022.9955647.

[19] G. M. V. Gil, E. O. H. Catata, J. C. C. Ccarita, J. G. Cardoso, A. J. S. Filho, and J. L. Azcue-Puma, "Digital controller design for interleaved boost converter in photovoltaic system," in *2016 12th IEEE International Conference on Industry Applications (INDUSCON)*, Nov. 2016, pp. 1–8. doi: 10.1109/INDUSCON.2016.7874598.

[20] R. B. A. Cunha, S. G. Di Santo, A. J. Sguarezi Filho, and F. F. Costa, "Finite control set applied to the current control of interleved boost converter of PV systems," in *2017 IEEE 6th International Conference on Renewable Energy Research and Applications (ICRERA)*, Nov. 2017, vol. 2017-Janua, pp. 580–584. doi: 10.1109/ICRERA.2017.8191127.

[21] G. M. Vargas-Gil, J. C. Colque, A. J. Sguarezi, and R. M. Monaro, "Sliding Mode plus PI Control applied in PV Systems Control," *2017 6th Int. Conf. Renew. Energy Res. Appl. ICRERA 2017*, vol. 2017-Janua, pp. 562–567, 2017, doi: 10.1109/DISTRA.2017.8191124.

[22] M. Ali, A. Krama, and S. S. Refaat, "A Robust Grid-Tied PV System based Super-Twisting Integral Sliding Mode Control," in *2021 10th International Conference on Renewable Energy Research and Application (ICRERA)*, Sep. 2021, pp. 402–407. doi: 10.1109/ICRERA52334.2021.9598701.

[23] S. Ouchen, M. Benbouzid, F. Blaabjerg, A. Betka, and H. Steinhart, "Direct Power Control of Shunt Active Power Filter Using Space Vector Modulation Based on Supertwisting Sliding Mode Control," *IEEE J. Emerg. Sel. Top. Power Electron.*, vol. 9, no. 3, pp. 3243–3253, Jun. 2021, doi: 10.1109/JESTPE.2020.3007900.

[24] D. E. O. Mohamed Cherif, A. Chebabhi, A. Kessal, M. F. Benkhoris, and M. Defdaf, "Super-Twisting Sliding Mode Control of Interleaved Boost Converter Based Photovoltaic Applications," in *2022 International Conference of Advanced Technology in Electronic and Electrical Engineering (ICATEEE)*, Nov. 2022, pp. 1–5. doi: 10.1109/ICATEEE57445.2022.10093715.

[25] E. M. G. Rodrigues, R. Melício, V. M. F. Mendes, and J. P. S. Catalão, "Simulation of a solar cell considering single-diode equivalent circuit mode," *Renew. Energy Power Qual. J.*, vol. 1, no. 9, pp. 369–373, May 2011, doi: 10.24084/repqj09.339.

[26] D. E. O. Mohamed Cherif, A. Chebabhi, and A. Kessal, "An Integral-Backstepping Controller for Interleaved Boost Converter based on Photovoltaic Systems," vol. 71, no. 1, pp. 13–21, 2023, doi: 10.46904/eea.23.71.1.1108002.

[27] I. Sami, S. Ullah, A. Basit, N. Ullah, and J. S. Ro, "Integral super twisting sliding mode based sensorless predictive torque control of induction motor," *IEEE Access*, vol. 8, pp. 186740–186755, 2020, doi: 10.1109/ACCESS.2020.3028845.

[28] S. Mirjalili, S. M. Mirjalili, and A. Lewis, "Grey Wolf Optimizer," *Adv. Eng. Softw.*, vol. 69, pp. 46–61, Mar. 2014, doi: 10.1016/j.advengsoft.2013.12.007.

[29] J.-S. Wang and S.-X. Li, "An Improved Grey Wolf Optimizer Based on Differential Evolution and Elimination Mechanism," *Sci. Rep.*, vol. 9, no. 1, p. 7181, May 2019, doi: 10.1038/s41598-019-43546-3.